블랙홀 쌍성의 형성과 진화

배영복 (기초과학연구원)

2022. 07. 29.

2022 수치상대론 및 중력파 여름학교

Introduction

Introduction

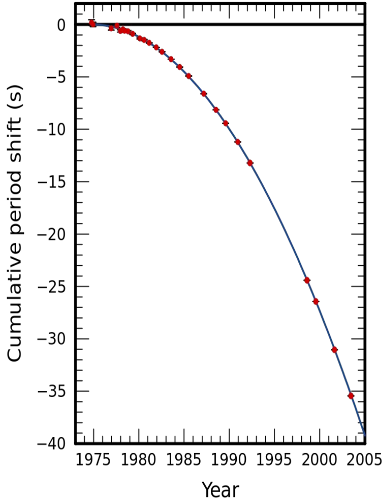

https://en.wikipedia.org/wiki/Hulse%E2%80%93Taylor_binary#/media/File:PSR_B1913+16_period_shift_graph.svg

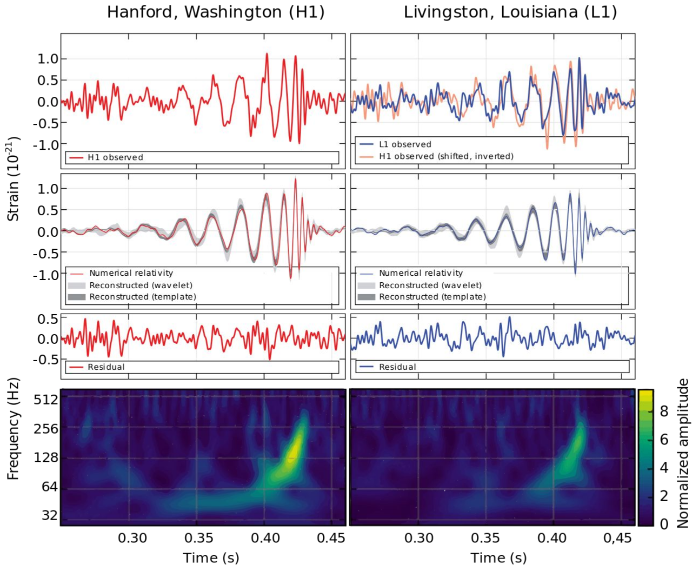

https://en.wikipedia.org/wiki/First_observation_of_gravitational_waves#/media/File:LIGO_measurement_of_gravitational_waves.svg

- Gravitational-Waves (GWs)
  - Ripples of spacetime curvature that propagate as waves
  - Indirect detection - PSR 1913+16 (Hulse & Taylor 1974, Weisberg & Taylor 2005)
  - Direct detection - GW150914 by aLIGO
  - Multi-messenger astronomy

Introduction

- Black hole (BH)
  - Solution of Einstein equation
  - Schwarzschild (1916), Kerr (1963)
  - Observations
    - X-ray binaries
    - Quasar
    - Stars orbiting Sagittarius A*
    - Gravitational waves
    - EHT
    - ...

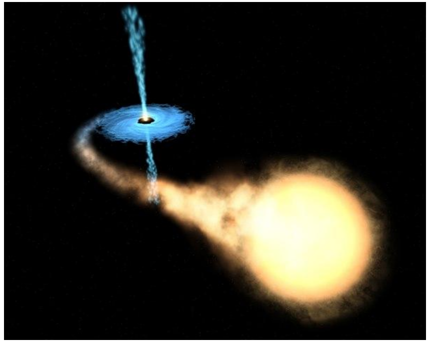

Wikipedia: X-ray binary

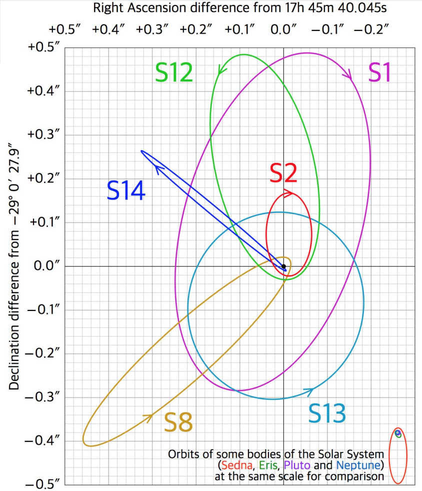

Wikipedia: Sagittarius A*

Wikipedia: Quasar

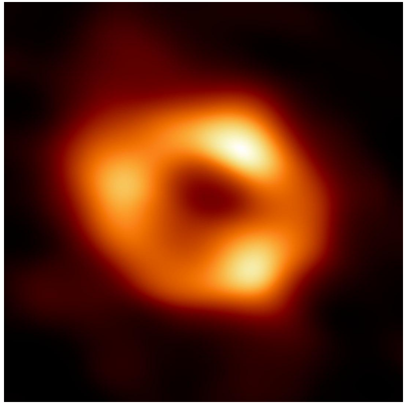

https://www.eso.org/public/images/eso2208-eht-mwa/

Introduction

- Black hole (BH)
  - Stellar evolution
    - Initial mass function of stars, metallicity, mass gap
  - Primordial
    - Early universe, Dark matter
  - Merger of neutron stars
  - Supermassive
    - M-σ relation
  - Intermediate mass

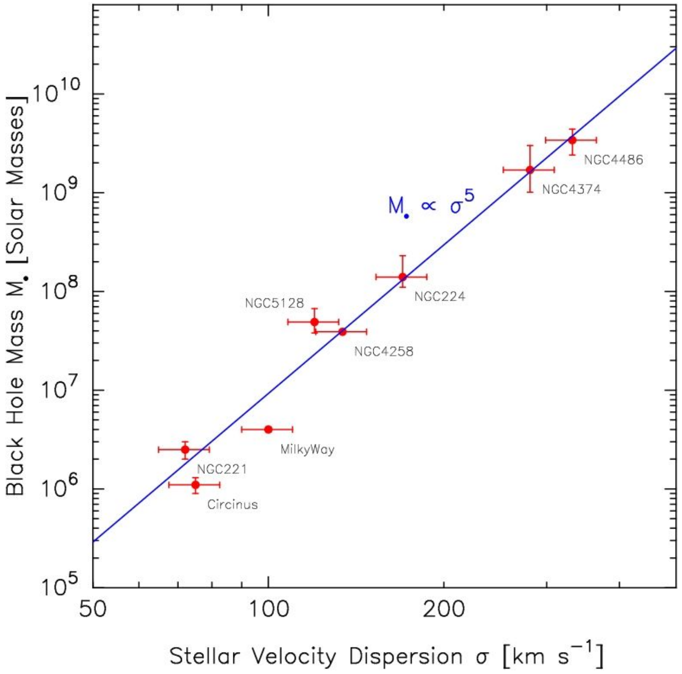

https://en.wikipedia.org/wiki/M%E2%80%93sigma_relation#/media/File:Msigma.jpg

GW sources

- GRB/Supernova, Spinning Neutron star, Cosmological sources, ...
- Compact Binary Coalescence (CBC)
  - Black hole, Neutron star
  - Strong signal
  - Detectable frequency for current GW detectors
  - Binary black hole (BBH)
    - Predictable wave forms
    - Inspiral-Merger-Ringdown
  - About 90 sources are detected.

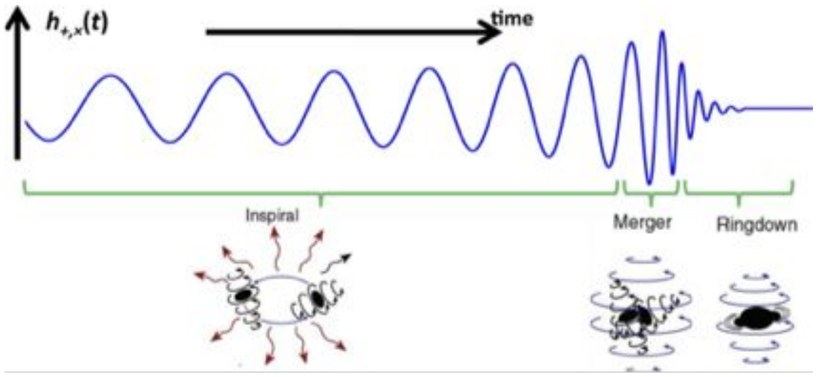

Inspiral-Merger-Ringdown (M. Favata, SXS, K. Thorne)

Formation of binary black hole

Field

- Galactic disk
- Evolution of stellar binary
- Common envelope phase

NGC 4414

The Hubble Heritage Team (AURA/STScI/NASA) NASA Headquarters - Greatest Images of NASA (NASA-HQ-GRIN) - http://nix.larc.nasa.gov/info;jsessionid=1sl2so6lc9mab?id=GPN-2000-000933&orgid=12 http://imgsrc.hubblesite.org/hu/db/images/hs-1999-25-a-full_tif.tif

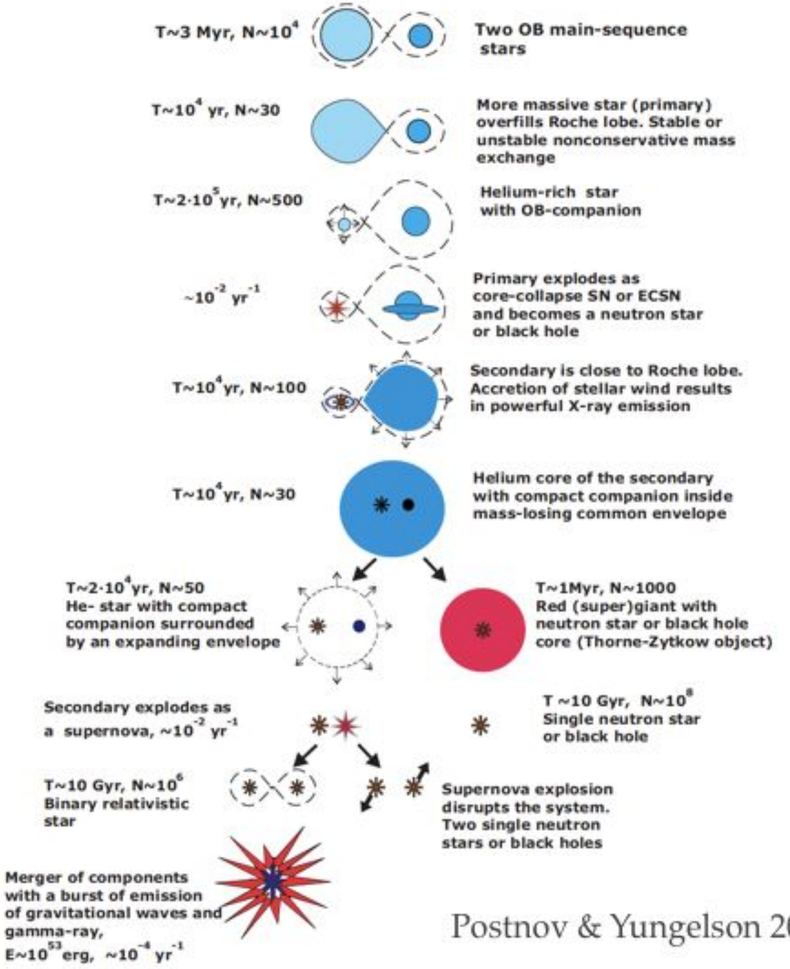

Postnov & Yungelson 2014

Figure 7: Evolutionary scenario for the formation of neutron stars or black holes in close binaries. T is the typical time scale of an evolutionary stage, N is the estimated number of objects in the given evolutionary stage.

Star cluster

M80 (NGC 6093)

NASA, The Hubble Heritage Team, STScI, AURA - Great Images in NASA Description

Nuclear star cluster of Milky Way

Stefan Gillessen, Reinhard Genzel, Frank Eisenhauer - http://www.eso.org/public/outreach/press-rel/pr-2008/pr-46-08.html

Dynamical evolution of star cluster

- Core collapse
  - Gravothermal instability
  - Negative heat capacity of self-gravitating system
  - Dense core - more encounters
  - Binary heating
- Mass segregation
  - Equipartition of kinetic energy
  - Dynamical friction
  - Massive components to center
- Evaporation

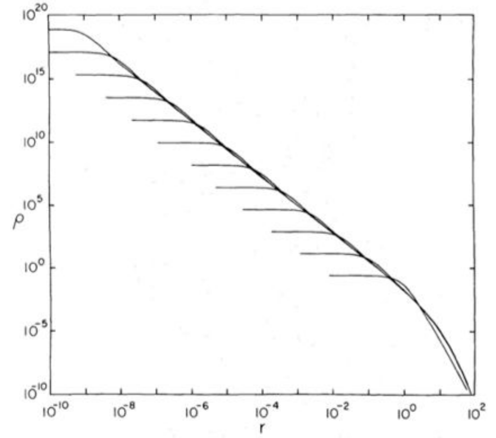

Core collapse (Cohn 1980)

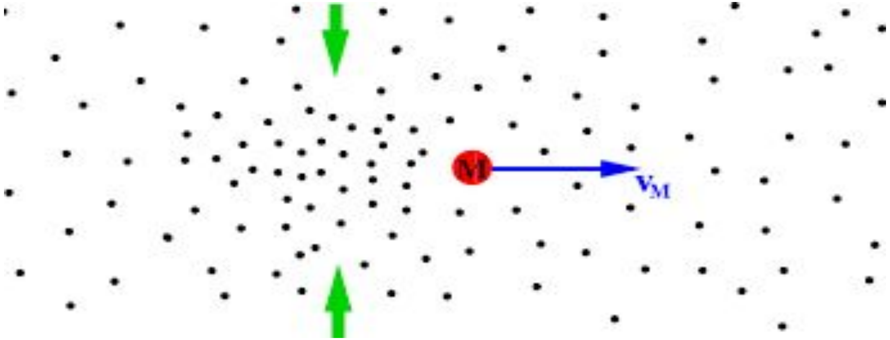

http://www.astro.yale.edu/vdbosch/astro610_lecture14.pdf

Dynamical evolution of cluster

- Binary formation
    - Dynamical formation through the interaction in the central region of star cluster
    - Tidal capture
        - almost no deformation in compact stars
    - Three-body process
    - Dynamical (Gravitational wave) capture

Three-body process

https://imgur.com/gallery/OkUBjPu

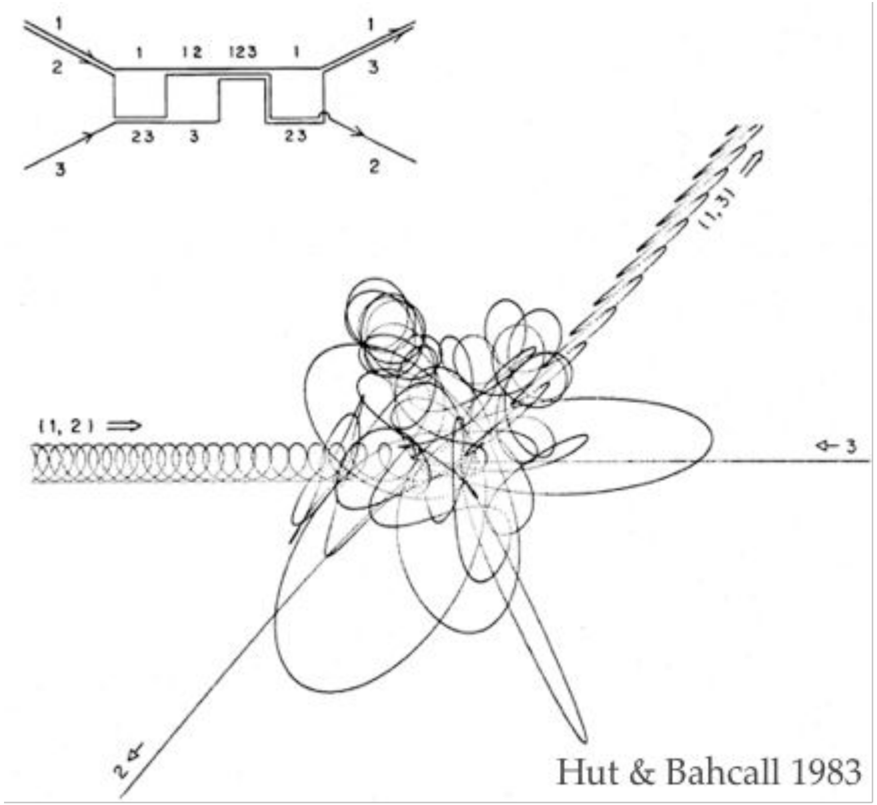

Dynamical capture

- Gravitational radiation driven capture (GR capture), or Gravitational wave capture (GW capture)
- Two body process
- Unbound orbit to bound orbit by emitting GWs
- Energy radiation > orbital energy

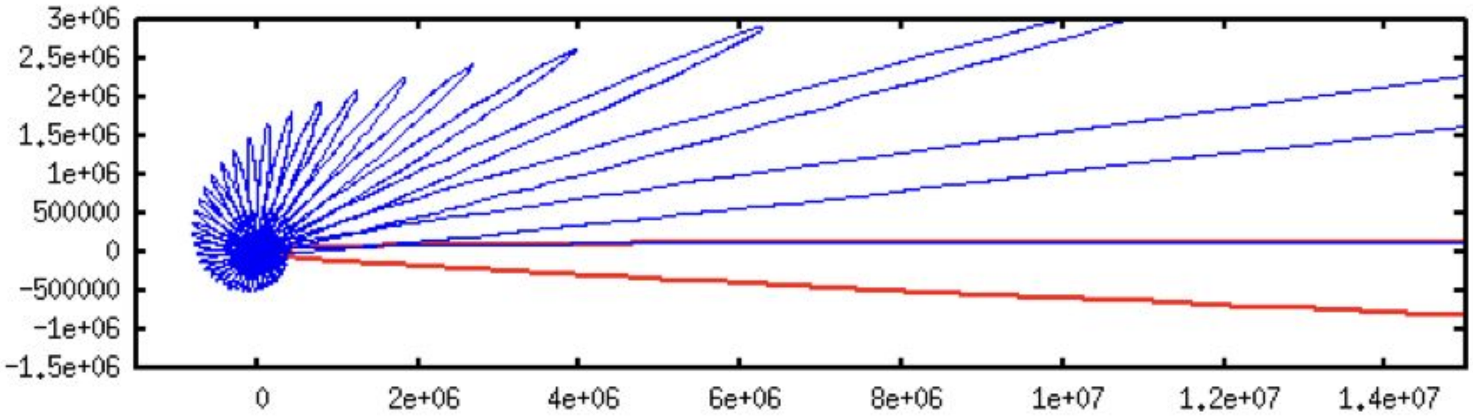

Dynamical capture

- Parabolic approximation (Quinlan & Shapiro 1989)
  - Hyperbolic orbit close to parabolic
  - Assume that GW radiation from hyperbolic orbit is the same with the parabolic orbit
  - Radiated energy (E_{rad}) from parabolic orbit → Hyperbolic orbit with $E \simeq E_{rad}$ can be captured.
  - Maximum periastron separation

$$r_{p,max} \simeq \left(\frac{85\pi\sqrt{2}G^{7/2}m_1 m_2 (m_1+m_2)^{3/2}}{12c^5 |v_1 - v_2|^2} \right)^{2/7}$$
$$\simeq 190 \text{ km} \left(\frac{\mu}{0.7M_\odot} \right)^{2/7} \left(\frac{m_1+m_2}{2.8M_\odot} \right)^{5/7} \left(\frac{|v_1-v_2|}{10^3 \text{km/s}} \right)^{-4/7}$$

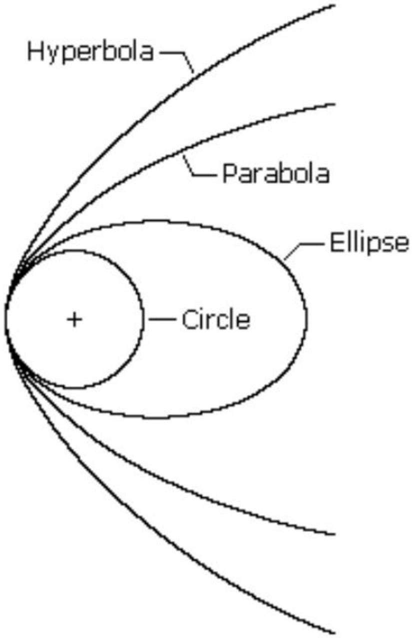

Three-body process vs. Dynamical capture

- Formation rate of three-body process

$$\dot{n}_{3b} = \frac{dn_{3b}}{dt} \simeq Cn^3 \frac{(Gm)^5}{\sigma^9}$$

- Formation rate of dynamical capture

$$\dot{n}_{cap} = \frac{dn_{cap}}{dt} = \frac{1}{2} n^2 \langle \Sigma_{cap} v_{rel} \rangle \qquad \Sigma_{cap} \simeq 17 \frac{G^2 m^2}{c^{10/7} v_\infty^{18/7}}$$

$$\rightarrow \frac{\dot{n}_{cap}}{\dot{n}_{3b}} \simeq 0.38 \left(\frac{10^5 \mathrm{pc}^{-3}}{n} \right) \left(\frac{10 \mathrm{M}_\odot}{m} \right)^3 \left(\frac{\sigma}{10 \mathrm{km/s}} \right)^{52/7}$$

Dynamical evolution of cluster

- Hardening of binary
- Escape from the star cluster

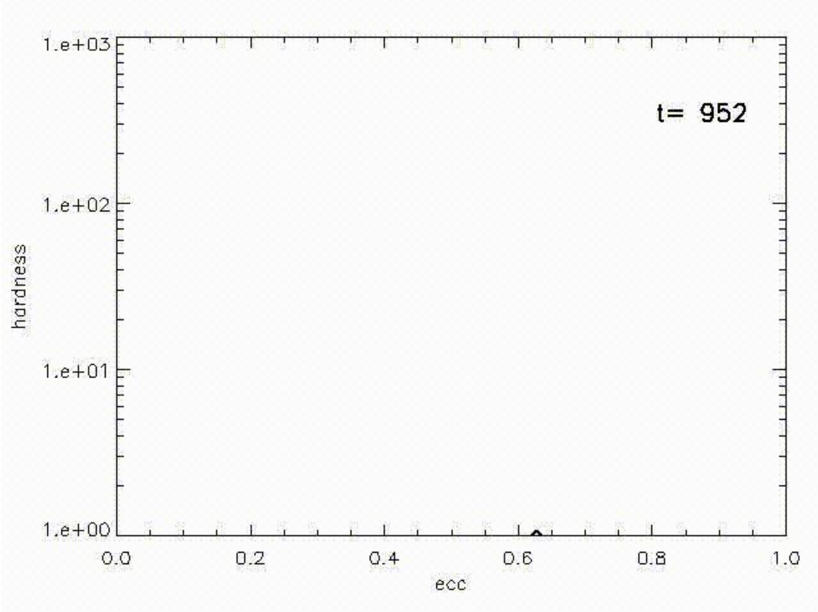

- **Dynamical evolution of cluster and binary formation**

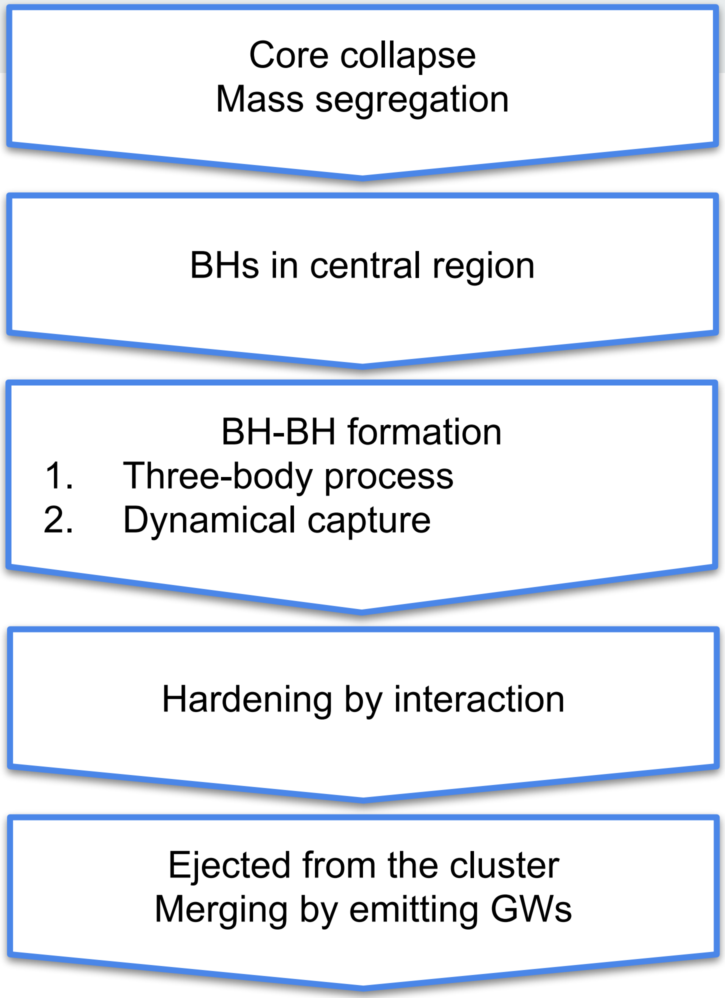

N-body

- Dynamical system of particles
    - stars, galaxies, atoms, molecules, human activities, …
- Numerical approach is required for N ≥ 3
- Direct N-body: $O(N^2)$ forces
- Tree method: Octree (Barnes-Hut algorithm), O(N log N)
- Particle mesh: mesh of density, Cloud-in-Cell method

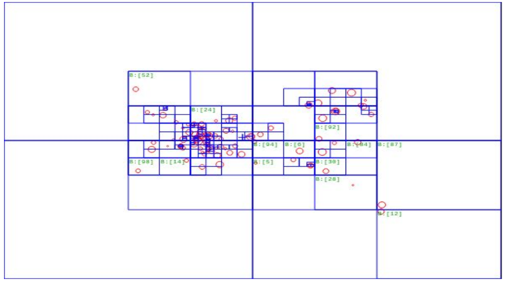

Barnes-Hut tree in 2D

(https://en.wikipedia.org/wiki/Barnes%E2%80%93Hut_simulation#/media/File:2D_Quad-Tree_partitioning_of_100_bodies.png)

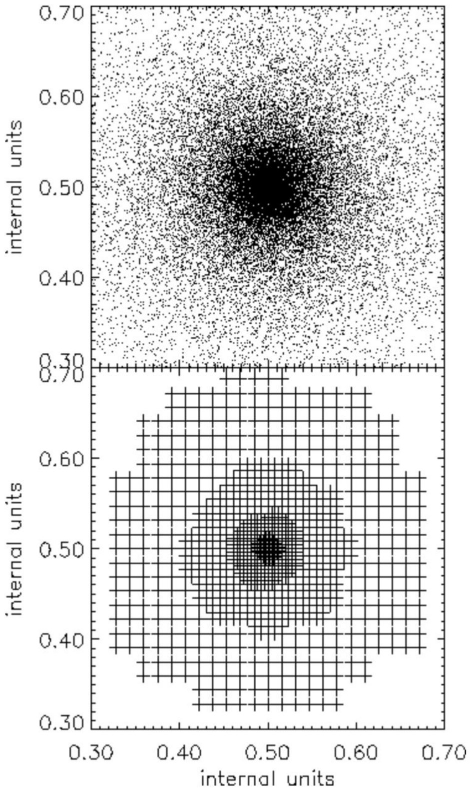

https://astronomy.swin.edu.au/sao/guest/knebe/#mlapmref

N-body

- NBODY6
    - https://people.ast.cam.ac.uk/~sverre/web/pages/nbody.htm
    - https://github.com/nbodyx/Nbody6
- Hermite integrator: predictor-corrector
- Individual timestep, block time step
- Ahmad-Cohen neighbor scheme: regular, irregular acceleration
- Regularization
- Various initial density profile, stellar evolution, stellar binary evolution, primordial binary, …
- GPU

- Dynamical evolution of star clusters and the formation of BBHs
    - Stars, NSs, and BHs are evenly mixed initially, but BHs sink toward center in early phase.
    - NSs fall to the center after the BHs are exhausted.
    - 30% of BHs are ejected in binary.
    - BH-NS binaries are rare.

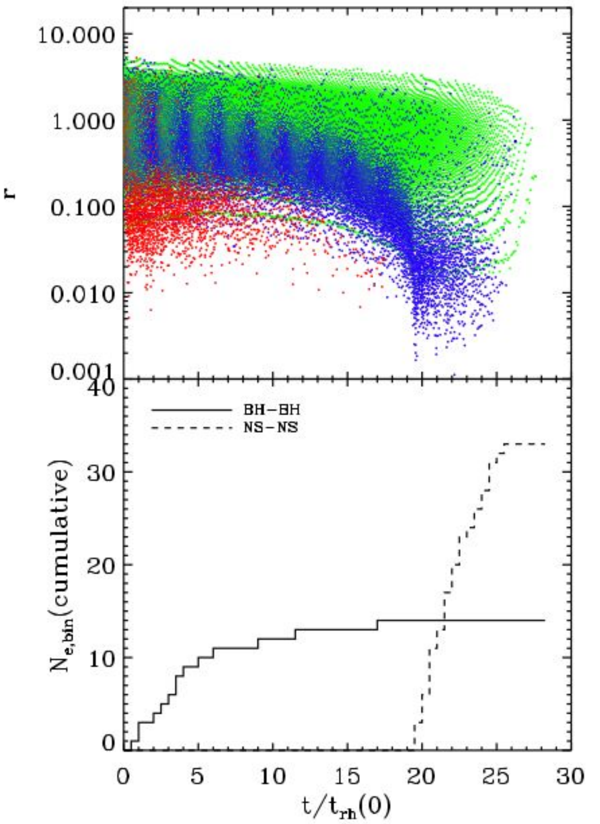

Figure 2. The upper panel: the distance of each mass component from the cluster centre is plotted against time. The total number of particles in the model is 50k, including 250 NSs and 100 BHs (model: A50kBN). Green, blue and red dots stand for the mean distance obtained from adjacent 200 ordinary stars, 4 NSs and 2 BHs, respectively. The lower panel: the cumulative number of ejected BH–BH or NS–NS binaries over time obtained from the same model.

Bae et al. (2014), Park et al. (2017)

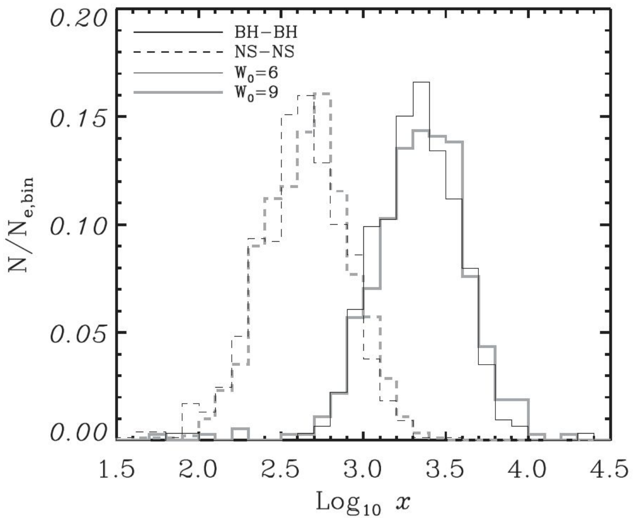

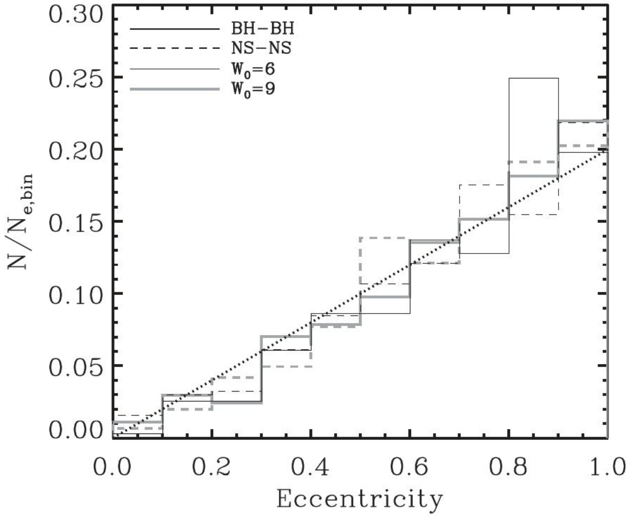

- Properties of ejected binaries
  - Tightly bound
  - High eccentricity
  - Low mass ratio

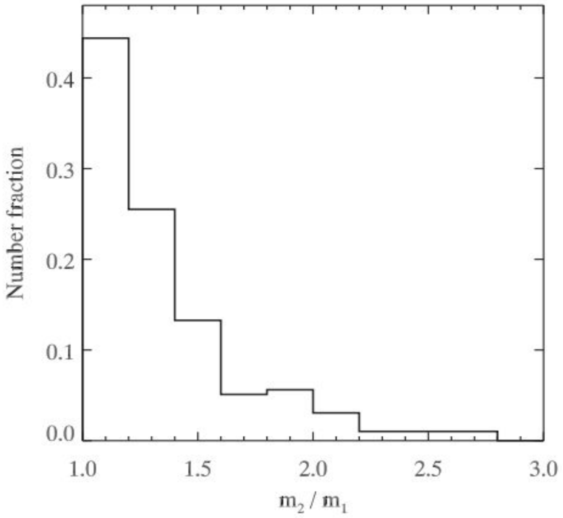

Bae et al. (2014), Park et al. (2017)

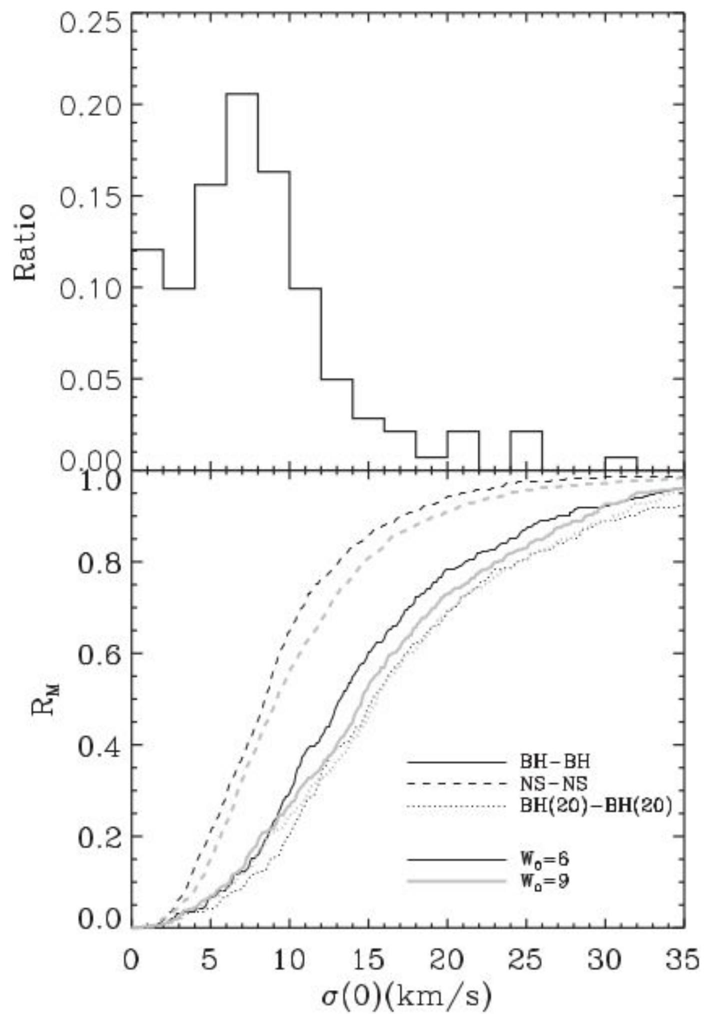

- Merger rate by considering of real globular clusters
  - Merger rate after the ejection depends on the central velocity of the cluster.
  - Merger rate of BBH is about 6.5 yr^{-1} Gpc^{-3}.
  - NS-NS binaries that are formed dynamically in the cluster are rare.

Bae et al. (2014), Park et al. (2017)

Evolution of binary black hole

Evolution Phase

- Inspiral - post-Newtonian, ...
- Merger - Numerical relativity
- Ringdown - Perturbation theory

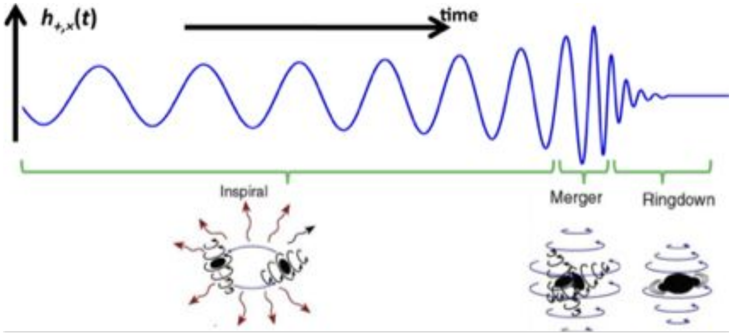

Inspiral-Merger-Ringdown (M. Favata, SXS, K. Thorne)

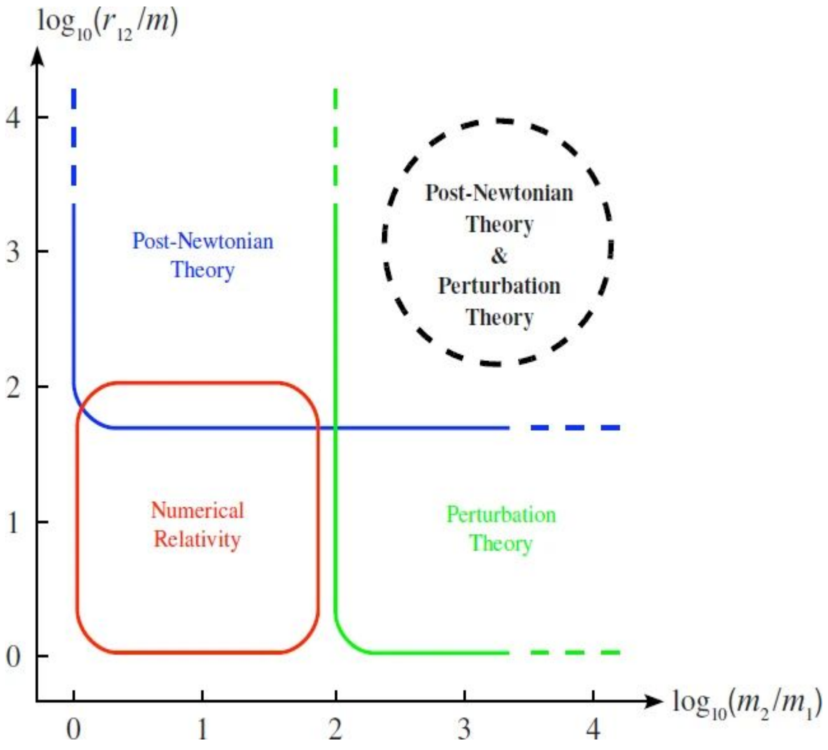

Blanchet, L. 2014, Living Reviews in Relativity, 17, 2

Peters & Mathews (1963)

PHYSICAL REVIEW VOLUME 131, NUMBER 1 1 JULY 1963

Gravitational Radiation from Point Masses in a Keplerian Orbit

P. C. PETERS* AND J. MATHEWS
California Institute of Technology, Pasadena, California

(Received 18 January 1963)

The gravitational radiation from two point masses going around each other under their mutual gravitational influence is calculated. Two different methods are outlined; one involves a multipole expansion of the radiation field, while the other uses the inertia tensor of the source. The calculations apply for arbitrary eccentricity of the relative orbit, but assume orbital velocities are small. The total rate, angular distribution, and polarization of the radiated energy are discussed.

Peters (1964)

PHYSICAL REVIEW VOLUME 136, NUMBER 4B 23 NOVEMBER 1964

Gravitational Radiation and the Motion of Two Point Masses

P. C. PETERS*†
California Institute of Technology, Pasadena, California

(Received 2 July 1964)

The expansion of the field equations of general relativity in powers of the gravitational coupling constant yields conservation laws of energy, momentum, and angular momentum. From these, the loss of energy and angular momentum of a system due to the radiation of gravitational waves is found. Two techniques, radiation reaction and flux across a large sphere, are used in these calculations and are shown to be in agreement over a time average. In the nonrelativistic limit, the energy and angular momentum radiation and angular distributions are expressed in terms of time derivatives of the quadrupole tensor Q_{ij}. These results are then applied to a bound system of two point masses moving in elliptical orbits. The secular decays of the semimajor axis and eccentricity are found as functions of time, and are integrated to specify the decay by gravitational radiation of such systems as functions of their initial conditions.

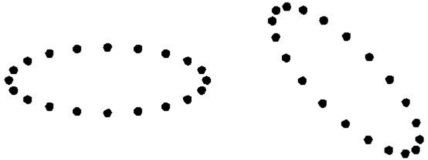

Inspiral

- Two polarization amplitudes of GWs

$$h_+ = \frac{G^{5/3}}{c^4}\frac{2}{r}(1+\cos^2 i)(\pi f M)^{2/3}\mu\cos(2\pi f t)$$

$$h_\times = \frac{G^{5/3}}{c^4}\frac{4}{r}\cos i(\pi f M)^{2/3}\mu\sin(2\pi f t)$$

$$h = (\langle h_+^2\rangle + \langle h_\times^2\rangle)^{1/2} = \left(\frac{32}{5}\right)^{1/2}\frac{G^{5/3}}{c^4}\frac{M_c^{5/3}}{r}(\pi f)^{2/3}$$

i : inclination angle
f : GW frequency
$\mu = \frac{m_1 m_2}{M}$: reduced mass
$M_c = \mu^{3/5}M^{2/5}$: chirp mass

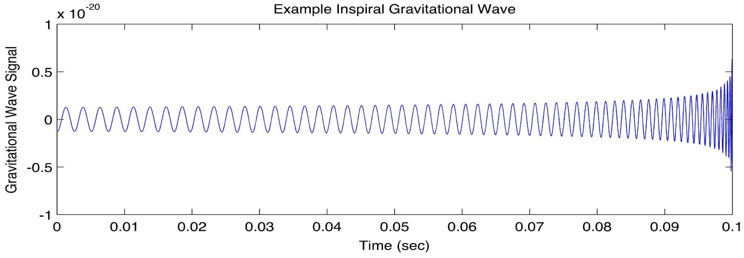

A. Stuver/LIGO, https://www.ligo.org/science/GW-Inspiral.php

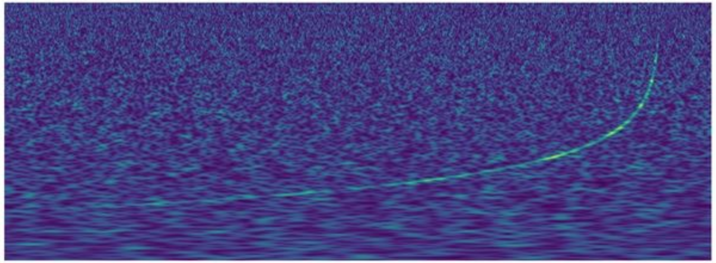

Credit: LSC/Alex Nitz, https://www.ligo.caltech.edu/WA/image/ligo20171016f

Inspiral

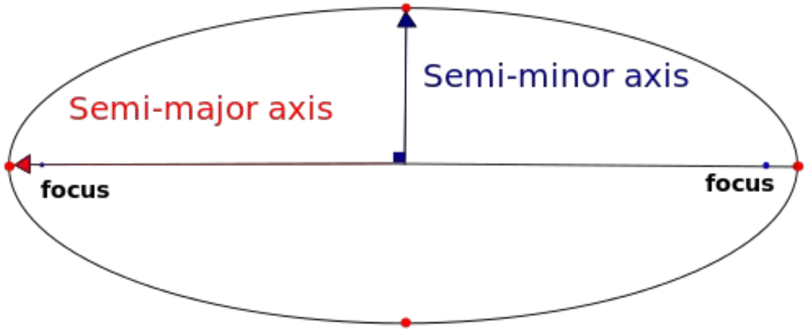

- Energy & Angular momentum radiation (Peters 1964)

$$\left\langle \frac{dE}{dt} \right\rangle = -\frac{32}{5} \frac{G^4 m_1^2 m_2^2 (m_1 + m_2)}{c^5 a^5 (1-e^2)^{7/2}} \left(1 + \frac{73}{24} e^2 + \frac{37}{96} e^4\right)$$

$$\left\langle \frac{dL}{dt} \right\rangle = -\frac{32}{5} \frac{G^{7/2} m_1^2 m_2^2 (m_1 + m_2)^{1/2}}{c^5 a^{7/2} (1-e^2)^2} \left(1 + \frac{7}{8} e^2\right)$$

a : semimajor axis
e : eccentricity

Inspiral

- Semi-major axis & eccentricity (Peters 1964)

$$\left\langle \frac{da}{dt} \right\rangle = -\frac{64}{5}\frac{G^3 m_1 m_2 (m_1 + m_2)}{c^5 a^3 (1-e^2)^{7/2}} \left(1 + \frac{73}{24}e^2 + \frac{37}{96}e^4\right)$$

$$\left\langle \frac{de}{dt} \right\rangle = -\frac{304}{15} e \frac{G^3 m_1 m_2 (m_1 + m_2)}{c^5 a^4 (1-e^2)^{5/2}} \left(1 + \frac{121}{304}e^2\right)$$

- Circularization

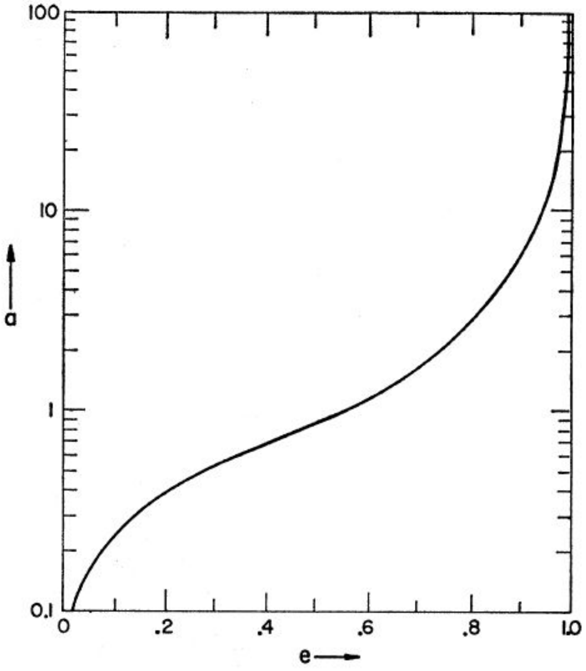

Inspiral (Moore et al. 2015)

$$h(t) = \sqrt{2} h_0 \cos \phi(t)$$

- Fourier Transform $\tilde{h}(f) \simeq \frac{h_0}{\sqrt{2\dot{f}}} = \frac{2c}{r}\left(\frac{5G\mu}{96c^3}\right)^{1/2}\left(\frac{GM}{\pi^2 c^3}\right)^{1/3} f^{-7/6}$
- Power Spectral density $\sqrt{S_n(f)} = h_n(f) f^{-1/2}, \quad \sqrt{S_h(f)} = 2f^{1/2}|\tilde{h}(f)|$
- Characteristic strain $h_n(f)^2 = f S_n(f), \quad h_c(f)^2 = 4f^2|\tilde{h}(f)|^2$
- Signal to noise ratio $\rho^2 = \int_0^\infty df \frac{4|\tilde{h}(f)|^2}{S_n(f)} = \int_{-\infty}^{\infty} d(\log f) \left[\frac{h_c(f)}{h_n(f)}\right]^2$

Inspiral

- Innermost Stable Circular Orbit (ISCO)
- ISCO of test particle in Schwarzschild metric

$$r_{ISCO} = \frac{6GM}{c^2}$$

- Highest GW frequency of inspiral phase

$$f_{ISCO,GW} = \frac{1}{\pi}\left(\frac{1}{6}\right)^{3/2} \frac{c^3}{G(m_1 + m_2)} \simeq \frac{4396}{M/M_\odot}\text{Hz}$$

- Spin, Comparable mass, ...

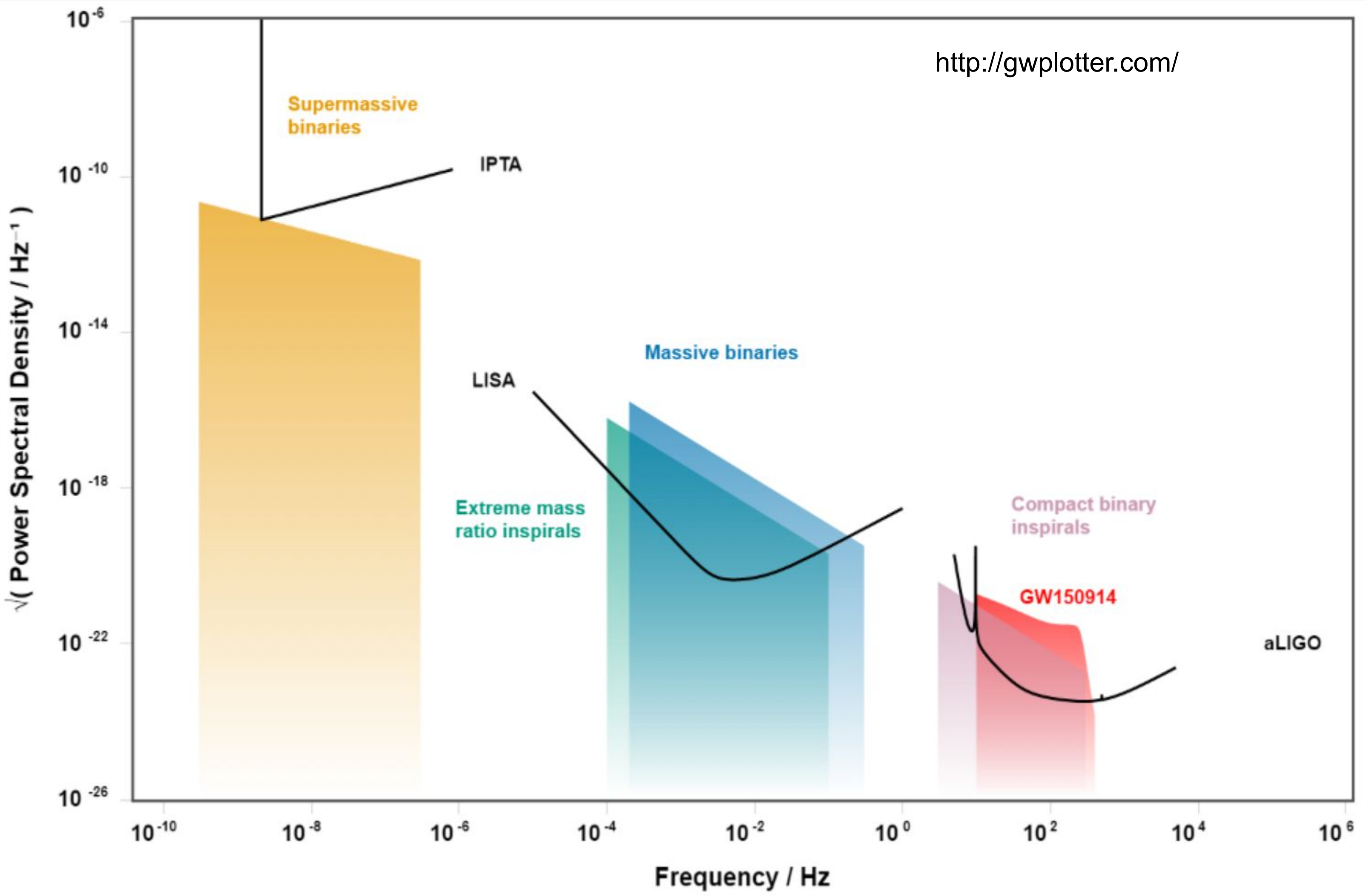
http://gwplotter.com/
Supermassive binaries
IPTA
LISA
Massive binaries
Extreme mass ratio inspirals
Compact binary inspirals
GW150914
aLIGO
√(Power Spectral Density / Hz⁻¹)
10 -6
10 -10
10 -14
10 -18
10 -22
10 -26
10 -10
10 -8
10 -6
10 -4
10 -2
10 0
10 2
10 4
10 6
Frequency / Hz

Inspiral

- Orbit

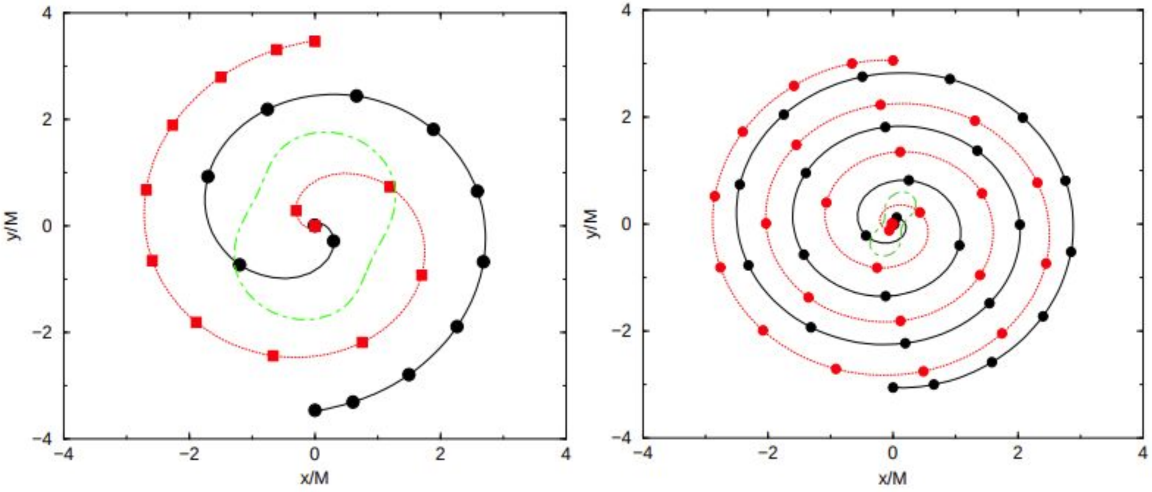

Campanelli et al. (2006)
Orbits with anti-aligned (left) and aligned (right) spins with the direction of orbital angular momentum

Merger

- GW emission peak
- Recoil (Kick)
  - Asymmetric GW emission
  - Unequal mass
  - Spin
  - Up to ~10,000 km/s (Healy et al. 2009)

Campanelli et al. (2007)

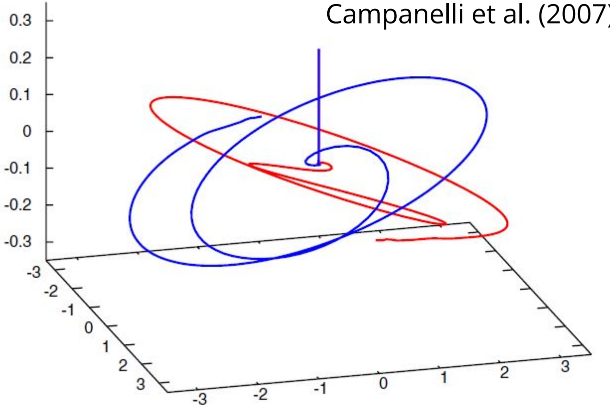

FIG. 4 (color online). The three-dimensional trajectories of the punctures showing the orbital precession and the final recoil for the SP2 configuration. Note that the scale of the z axis is $1/10$ that of the x and y axes.

Ringdown

- Ringing of merged black hole
- Damping vibration with emitting GWs
- Quasi-normal mode (Berti et al. 2006)

$$h(t) \sim A \exp[2\pi i (f_R + i f_I) t]$$

$$f_R + i f_I \text{ : quasinormal mode frequency}$$

$$Q = \frac{f_R}{2 f_I} \text{ : quality factor}$$

$$f_{qnm} = \frac{c^3}{2\pi G M_T} f_R \sim 3.2 \left(\frac{10 M_\odot}{M_T} \right) f_R [\mathrm{kHz}]$$

Shinkai et al. (2017)

Observation (GWTC-3) & simulation of BBHs

Observation of GWs

- GWTC-1 (Gravitational-Wave Transient Catalog)
  - O1 (Sep. 12, 2015 - Jan. 19, 2016)
    - first detection of GWs
  - O2 (Nov. 30, 2016 - Aug. 25, 2017)
    - first detection of a binary neutron star inspiral
  - 11 GW candidates
- GWTC-2, GWTC-2.1
  - O3a (Apr. 01, 2019 - Oct. 01, 2019)
  - 44 GW candidates
- GWTC-3
  - O3b (Nov. 01, 2019 - Mar. 27, 2020)
  - 35 GW candidates

Masses in the Stellar Graveyard

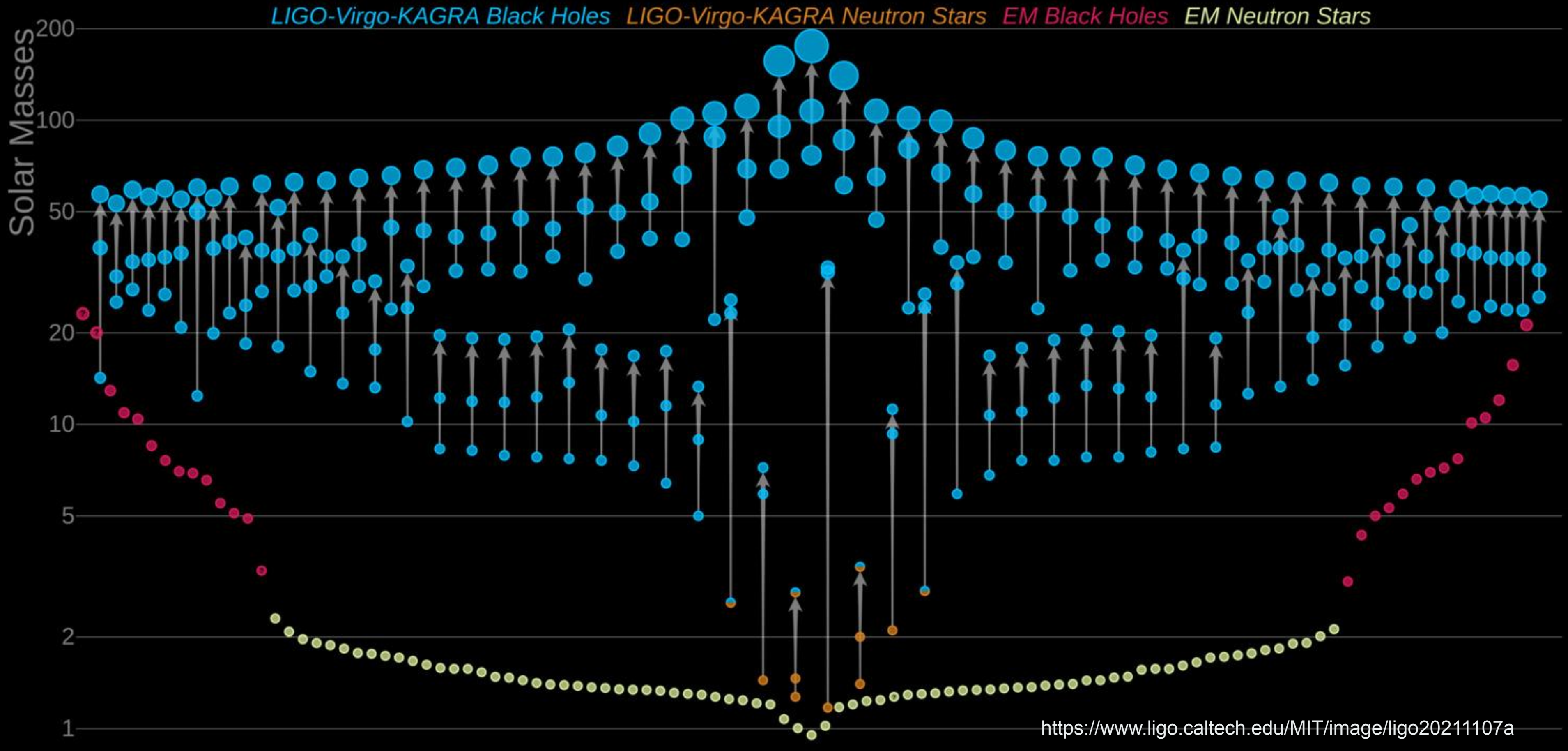

https://www.ligo.caltech.edu/MIT/image/ligo20211107a

LIGO-Virgo-KAGRA | Aaron Geller | Northwestern

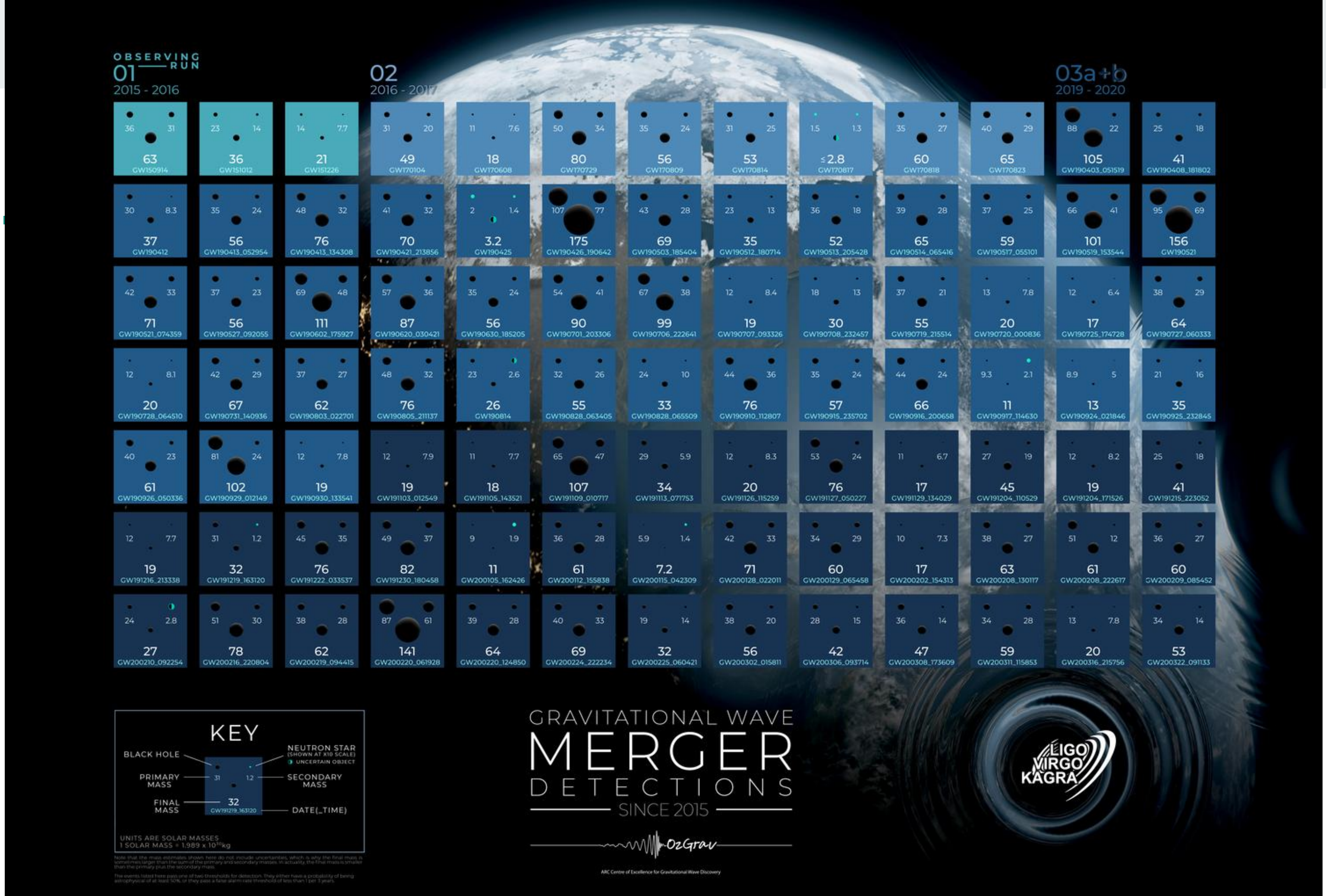

https://www.ligo.caltech.edu/MIT/image/ligo20211107b

Masses

- Best constrained binary parameters
- Lower and upper mass gap of BH
- Mass range of NS
- Total mass
  - Determines the highest frequency of GWs
  - lower (higher) mass systems merge at higher (lower) frequency
  - Influences the merger and ringdown signal
- Chirp mass
  - More precisely measured than the individual component masses
  - Influence on a CBC signal's frequency evolution
  - Phase evolution during inspiral to leading order
- Mass ratio
  - less precisely inferred from GWs than chirp mass or total mass
  - Phase evolution of inspiral at post-Newtonian order after the chirp mass
  - Most are close to equal-mass q~1

$$M = m_1 + m_2$$

$$\mathcal{M} = \frac{(m_1 m_2)^{3/5}}{(m_1 + m_2)^{1/5}}$$

$$q = m_2/m_1$$

Unambiguous BBHs in GWTC-3

- $m_2 > 3M_\odot$
- Highest & lowest chirp mass
  - GW200220_061928: $\mathcal{M} = 62^{+23}_{-15}\mathrm{M}_\odot$
  - GW191129_134029: $\mathcal{M} = 7.31^{+0.43}_{-0.28}\mathrm{M}_\odot$
- Highest & Lowest total mass
  - GW200220_061928: $M = 148^{+55}_{-33}\mathrm{M}_\odot \ (m_1 = 87^{+40}_{-23}\mathrm{M}_\odot, m_2 = 61^{+26}_{-25}\mathrm{M}_\odot)$
  - GW191129_134029: $M = 17.5^{+2.4}_{-1.2}\mathrm{M}_\odot \ (m_1 = 10.7^{+4.1}_{-2.1}\mathrm{M}_\odot, m_2 = 6.7^{+1.5}_{-1.7}\mathrm{M}_\odot)$
- Largest mass ratio
  - GW191113_071753: $q = m_2/m_1 = 0.202^{+0.490}_{-0.087}(m_1 = 29^{+12}_{-14}\mathrm{M}_\odot, m_2 = 5.9^{+4.4}_{-1.3}\mathrm{M}_\odot)$
- Mass range
  - Primary: $10.1^{+3.5}_{-1.4}\mathrm{M}_\odot \sim 87^{+40}_{-23}\mathrm{M}_\odot$
  - Secondary: $5.9^{+4.4}_{-1.3}\mathrm{M}_\odot \sim 61^{+26}_{-25}\mathrm{M}_\odot$

Potential NS binaries in GWTC-3

- $m_2 < 3M_\odot$
- NS-BH
  - GW191219_163120
  - GW200105_162426 (p_{astro}<0.5, but small FAR, outlier from background noise)
  - GW200115_042309
  - GW200210_092254 (NSBH? BBH?): $m_2 = 2.83^{+0.47}_{-0.42}\mathrm{M}_\odot$
- Matter effects are expected to modify the waveform, but they found no measurable matter effects.
- More extreme mass ratios
  - e.g., GW191219_163120: $q = 0.038^{+0.005}_{-0.004}, m_1 = 31.1^{+2.2}_{-2.8}\mathrm{M}_\odot, m_2 = 1.17^{+0.07}_{-0.06}\mathrm{M}_\odot$
  - challenging for waveform modeling
- Lowest total mass
  - GW200115_042309: $m_1 = 5.9^{+2.0}_{-2.5}\mathrm{M}_\odot, m_2 = 1.44^{+0.85}_{-0.29}\mathrm{M}_\odot$

Spins

- More difficult to measure than the masses
- Effective inspiral spin
  - approximately conserved throughout the inspiral
  - positive (negative) : net spin aligned (anti-aligned) with the orbital angular momentum

$$\chi_{\rm eff} = \frac{(m_1\vec{\chi_1} + m_2\vec{\chi_2}) \cdot \hat{L}_N}{M}$$

- Effective precession spin
  - in-plane spin component that contribute to spin precession
  - weakly constrained
  - Changes throughout the inspiral

$$\chi_p = \max\left\{\chi_{1,\perp}, \frac{q(4q+3)}{4+3q}\chi_{2,\perp}\right\}$$

- Typically, it is not possible to put strong constraints on individual components' spins, but when mass ratio is large, it may be possible to constrain the primary spin.

Spins in GWTC-3

- Spin orientation provide clues to its formation channel
  - Dynamically assembled binaries would have no preferred spin orientation. (negative χ_{eff} or large χ_p)
  - Binaries from isolated binary evolution are expected to have nearly aligned spins.
- Most of candidates are consistent with X_{eff}=0.
- More systems with X_{eff}> 0 than with X_{eff}< 0.
- High X_{eff}
  - GW200308_173609 with $\chi_{\rm eff} = 0.65^{+0.17}_{-0.21}$
- Most significant support for X_{eff}< 0
  - GW191109_010717: X_{eff}< 0 at 90% ($\chi_{\rm eff} = -0.29^{+0.42}_{-0.31}$)
  - GW200225_060421: X_{eff}< 0 at 85% ($\chi_{\rm eff} = -0.12^{+0.17}_{-0.28}$)
- X_p and component spin posteriors are usually broad and uninformative, except the cases with extreme mass ratios.
  - GW200208_222617: X_1≥0.29 at 90% probability, X_1>0.8 at 51% probability

Final Spins

- Final spin of the merger remnant χ_f
  - Determined by conservation of angular momentum
  - Receives contributions from both the orbital angular momentum at merger and the component spins
  - Equal mass, non-spinning BHs : χ_f ~0.7.
  - GW191219_163120: $\chi_\mathrm{f} = 0.14^{+0.06}_{-0.06}$
  - GW200208_222617: $\chi_\mathrm{f} = 0.91^{+0.03}_{-0.08}$

Distance

- Distance is inferred from the amplitude of the signal.
- Closest source
  - O3b: GW200105_162426 $D_L = 0.27^{+0.12}_{-0.11}\mathrm{Gpc}(z = 0.06^{+0.02}_{-0.02})$
- Farthest source
  - O3b: GW200220_061928 $D_L = 6.0^{+4.8}_{-3.1}\mathrm{Gpc}(z = 0.90^{+0.55}_{-0.40})$
  - GW190403_051519 (GWTC-2.1) $D_L = 8.00^{+5.88}_{-3.99}\mathrm{Gpc}$

Localization

- Most constrained localizations are obtained when all three observatories record a significant SNR.
- Crucial to multi-messenger follow-up
- Best sky localization in O3b
  - GW200208_130117: 30 deg^2 (90% credible) with all three detectors
- Best volume localization (distance + sky localization)
  - GW200202_154313 and GW200115_042309: 0.0024 Gpc^3 (90% credible)
  - These corresponds to two of the closest sources.
  - ~1500 and 5800 galaxies (K band)

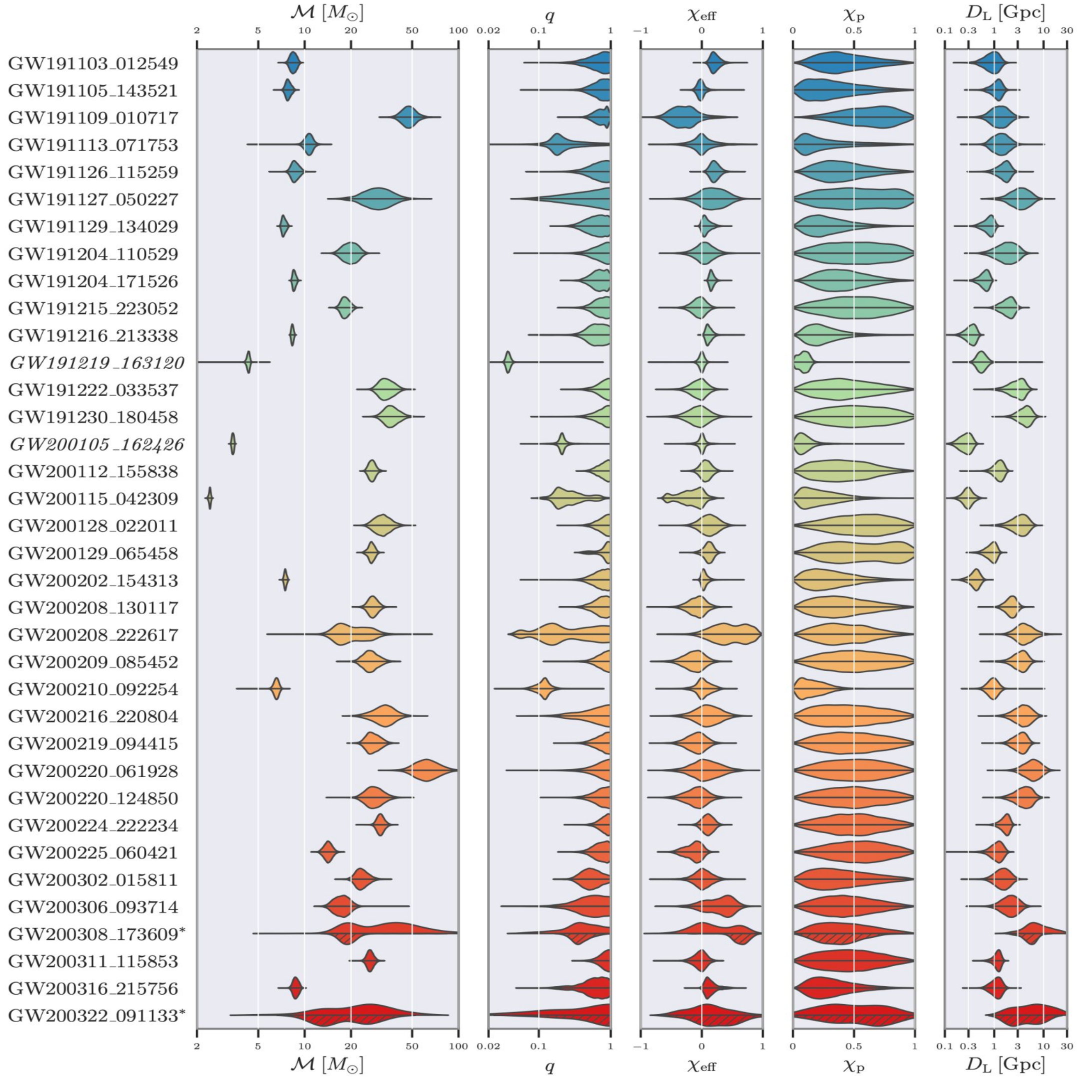

- Most candidates
  - are composed of comparable masses q~1.
  - have small effective inspiral spins.

Numerical Relativity

- Einstein Equations

$$G_{\mu\nu} \equiv R_{\mu\nu} - \frac{1}{2} g_{\mu\nu} R = \frac{8\pi G}{c^4} T_{\mu\nu}$$

  - Relation between geometry of spacetime and matter
- Numerical solution of Einstein equations
- Black holes, Neutron stars, Cosmology, …

Numerical Relativity

- 3+1 decomposition
  - 4 dimensional spacetime -> 3+1 dimension
  - Constraint equations
    - Hamiltonian constraint
    - Momentum constraint
  - Evolution equations
  - Gauge choice
    - Lapse and shift

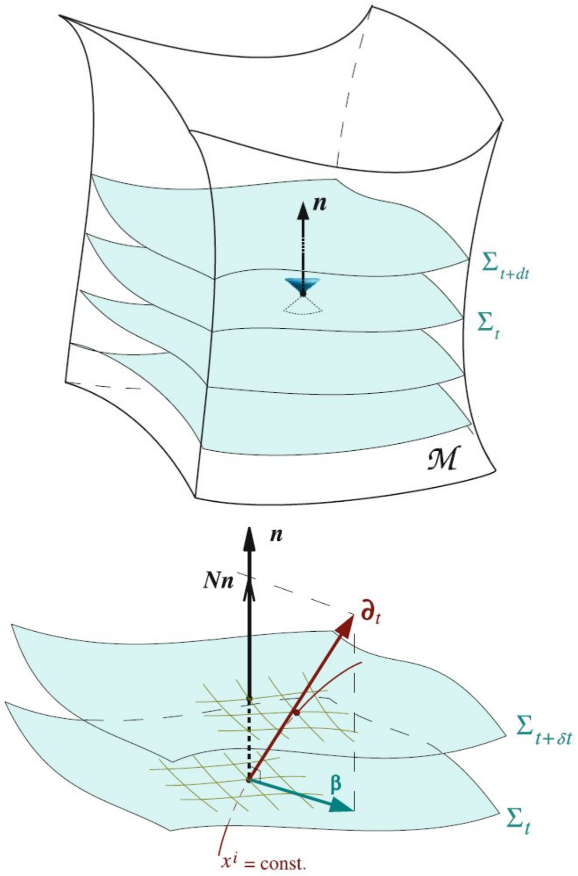

Gourgoulhon, E. 2012, 3+1 Formalism in General Relativity: Bases of Numerical Relativity, Lecture Notes in Physics, Volume 846

Standard 3+1 or ADM equations

Metric	$ds^2 = -\alpha^2 dt^2 + \gamma_{ij}(dx^i + \beta^i dt)(dx^j + \beta^j dt)$
Hamiltonian Constraint	$R + K^2 - K_{ij}K^{ij} = 16\pi\rho$
Momentum Constraint	$D_j(K^{ij} - \gamma^{ij}K) = 8\pi S^i$
Evolution equation of spatial metric	$\partial_t \gamma_{ij} = -2\alpha K_{ij} + D_i\beta_j + D_j\beta_i$
Evolution equation of extrinsic curvature	$\partial_t K_{ij} = \alpha(R_{ij} - 2K_{ik}K^k_j + KK_{ij}) - D_iD_j\alpha - 8\pi\alpha(S_{ij} - \frac{1}{2}\gamma_{ij}(S-\rho))$ $+ \beta^k\partial_k K_{ij} + K_{ik}\partial_j\beta^k + K_{kj}\partial_i\beta^k$
$\rho = n_a n_b T^{ab}, \quad S^i = -\gamma^{ij}n^a T_{aj}, \quad S_{ij} = \gamma_{ia}\gamma_{jb}T^{ab}, \quad S = \gamma^{ij}S_{ij}$	

Initial conditions

- Unlike Schwarzschild or Kerr, the initial condition of BBH cannot be given analytically.
- Conformal transverse-traceless decomposition (CTT)
  - Spatial metric (γ_{ij}) and extrinsic curvature (K_{ij}) on initial spatial slice
  - Bowen-York initial data
    - Conformally flat $\gamma_{ij} = \psi^4 \bar{\gamma}_{ij} = \psi^4 \eta_{ij}$
    - Maximal slicing $K = 0$
    - Zero transverse-traceless part of extrinsic curvature $\bar{A}^{ij}_{TT} = 0$
- Conformal thin-sandwich decomposition (CTS)
  - Spatial metric on two slices, or spatial metric and its time derivative

BBH simulation

- Time evolution schemes
  - Constrained schemes, Free evolution schemes
- BSSN scheme (Shibata and Nakamura 1995, Baumgarte and Shapiro 1999)
  - Most widely used evolution scheme
  - Long term stable evolution
- BBH simulation
  - Black hole excision (Pretorius 2005)
  - Puncture method (Baker et al. 2006, Campanelli et al. 2006)

Einstein Toolkit

- Collection of software components and tools for simulation and analysis for general relativistic phenomena
- Free and Open source (https://einsteintoolkit.org)
- Vacuum spacetime & Relativistic hydrodynamics
- Based on Cactus code
    - Flesh (central core) + Thorns (application module)
    - Over 100 thorns
- Initial condition, Mesh refinement, Wave extraction, …
- Regular updates (Riemann, released on May 31th, 2022)

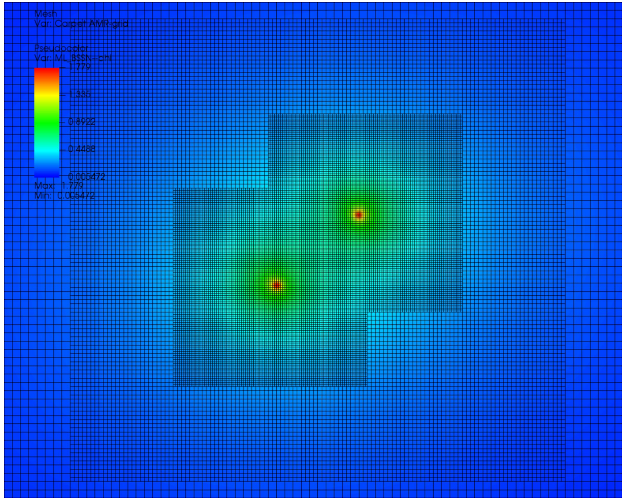

SUMMARY

- BBHs are the main targets of current GW detectors.
- BBHs can be formed dynamically in the central region of star clusters.
- BBHs can be studied from the observations and analytical/numerical methods.